European Journal of Radiology 117 (2019) 56–61

Contents lists available at ScienceDirect

European Journal of Radiology

journal homepage: www.elsevier.com/locate/ejrad

Research article

Susceptibility-weighted imaging provides complementary value to diffusion-weighted imaging in the differentiation between pyogenic brain abscesses, necrotic glioblastomas, and necrotic metastatic brain tumors

Ping-Hong Lai[a,b], Hsiao-Wen Chung[c], Hing-Chiu Chang[d], Jui-Hsun Fu[a], Po-Chin Wang[a], Shuo-Hsiu Hsu[a], Shu-Shong Hsu[e], Huey-Shyan Lin[f], Tzu-Chao Chuang[g,*]

[a] Department of Radiology, Kaohsiung Veterans General Hospital, Kaohsiung, Taiwan
[b] School of Medicine, National Yang-Ming University, Taipei, Taiwan
[c] Department of Electrical Engineering, National Taiwan University, Taipei, Taiwan
[d] Department of Diagnostic Radiology, The University of Hong Kong, Hong Kong
[e] Department of Neurosurgery, Kaohsiung Veterans General Hospital, Kaohsiung, Taiwan
[f] Department of Health-Business Administration, School of Nursing, Fooyin University, Kaohsiung, Taiwan
[g] Department of Electrical Engineering, National Sun Yat-Sen University, Kaohsiung, Taiwan

ARTICLE INFO

Keywords:
Apparent diffusion coefficient
Susceptibility weighted imaging
Intralesional susceptibility signal
Brain abscess
Glioblastoma
Metastasis

ABSTRACT

Purpose: The purpose of this retrospective study was to investigate the differentiation of abscess and necrotic tumors, using susceptibility-weighted imaging (SWI) and apparent diffusion coefficients (ADC) either separated or combined.

Methods: Imaging was performed on 26 patients with pyogenic brain abscesses, 31 patients with rim-enhancing glioblastomas, and 21 patients with rim-enhancing metastases. The degree of intralesional susceptibility signal (ILSS) was independently assessed by three observers. Average ADC in the lesion core was calculated. After receiver operating characteristic (ROC) analysis, the area under the ROC curve was compared using three different analytical models (ILSS, ADC, and ILSS-ADC combined) to differentiate abscess from the two rim-enhancing necrotic tumors.

Results: The ILSS-ADC combined model had greater area under the ROC curves than ILSS or ADC used alone. In this study, the ILSS-ADC combined model showed 100% diagnostic accuracy differentiating abscesses from glioblastoma. The ADC model and the ILSS-ADC combined model performed equally well in distinguishing abscesses from metastases.

Conclusion: It is concluded that SWI and ADC are complementary, and the combination of SWI and ADC may improve results compared with the use of only one model. Validation by an independent cohort is the next necessary step to broaden its applicability in routine clinical settings.

1. Introduction

Pyogenic brain abscesses, necrotic glioblastomas, and necrotic metastatic lesions frequently appear as rim-enhancing abnormalities on contrast-enhanced T1-weighted MR images, accompanied by surrounding edema. Although the pathological origins of these abnormalities are completely different, the similarity in their appearance on conventional MR imaging can prove to be a challenge during differential diagnosis based on imaging findings alone [1,2]. It is well known that the ADC value derived from diffusion-weighted imaging (DWI) complements the role of conventional MR imaging in the differentiation of abscesses from necrotic tumors, given that the ADC of the pus in the abscess cavities is generally low, whereas in tumor the ADC value in the necrotic core is often high [3–6]. However, exceptions are common. High ADC values similar to those found in necrotic tumors have been reported in 5%–21% of untreated abscesses [7,8]. Some necrotic glioblastomas, on the contrary, may show low ADC mimicking the DWI appearance of brain abscesses [8–11]. Therefore, it is hoped that the

Abbreviations: DWI, diffusion-weighted imaging; SWI, susceptibility-weighted imaging; ILSS, intralesional susceptibility signal; ROC curve, receiver operating characteristics curve; AUC, area under the ROC curve; KCC, Kendall's coefficient of concordance; ICC, intraclass correlation coefficient

* Corresponding author at: Department of Electrical Engineering, National Sun Yat-Sen University, 70 Lienhai Rd., Kaohsiung, 80424, Taiwan.
E-mail address: chuang@mail.ee.nsysu.edu.tw (T.-C. Chuang).

https://doi.org/10.1016/j.ejrad.2019.05.021
Received 7 March 2019; Received in revised form 22 May 2019; Accepted 28 May 2019
0720-048X/ © 2019 Elsevier B.V. All rights reserved.

search for new imaging techniques to assist in distinguishing brain abscess from necrotic glioblastomas and necrotic metastases shows promising potential for accurate differential diagnosis before treatment decisions [5,6].

In a past study, the presence of intralesional susceptibility signal (ILSS), a semi-quantitative index derived from susceptibility-weighted imaging (SWI), was demonstrated to contribute to the differential diagnosis of rim-enhancing masses [12]. The principles for assessment using SWI are based on findings of fine linear or dot-like low-signal-intensity structures within the lesions [13,14], which indicate the presence of paramagnetic substances [15,16] that may be associated with tumor necrosis, microhemorrhage, and tumor microvascularity. Consequently, we hypothesized in the current study that SWI may complement ADC in the differential diagnosis of rim-enhancing masses. For this purpose we conducted a detailed analysis by adopting the concept of ILSS using SWI integrated with ADC on patients with pyogenic brain abscesses, necrotic glioblastomas, and necrotic metastases.

2. Materials and methods

2.1. Study patients

This retrospective study included data from 78 patients who had MRI examinations between March 2009 and September 2013 with final diagnosis of brain abscess, necrotic glioblastoma, and necrotic metastasis. The inclusion criteria were rim-enhancing lesions on T1-weighted images following contrast administration, plus that they underwent both SWI and DWI. Written informed consents were obtained from all the patients included in this study. The current study was approved by our institutional review board. Demographic data has been summarized in Table 1. Of the 78 patients, 26 had pyogenic abscesses [age (mean ± SD) 51.3 ± 20.1 years; 19 males and 7 females], 31 had glioblastomas (age 60.3 ± 13.5 years; 17 males and 14 females), and 21 had metastases (age 57.7 ± 14.5 years; 11 males and 10 females). Primary metastatic tumors consisted of lung (n = 14), breast (n = 5), colon (n = 1), and hepatocellular carcinoma (n = 1). The abscess was diagnosed by culture of the pus and histopathology that revealed an area of cerebral necrotic inflammation and encapsulated by glial cells and fibroblasts. The glioblastoma was diagnosed by the histopathology showing nuclear atypia, increased mitotic activity, microvascular proliferation and necrosis of the astrocytic tumors. The histological appearance of metastasis depended on the primary tumor, and all had been pathologically proven with specimens taken via neurosurgical biopsy.

Table 1
Demographic data, ILSS grade and ADC value of abscesses, necrotic glioblastomas, and necrotic metastases.

	Brain lesion pathology		
	Abscess (n = 26)	Glioblastoma (n = 31)	Metastasis (n = 21)
Sex			
Male	19 (73.1%)	17 (54.8%)	11 (52.4%)
Female	7 (26.9%)	14 (45.2%)	10 (47.6%)
Age (years)	51.3 ± 20.1	60.3 ± 13.5	57.7 ± 14.5
ILSS grade [n (%)] [a]			
0	12 (46.2%)	1 (3.2%)	7 (33.3%)
1	11 (42.3%)	3 (9.7%)	4 (19.0%)
2	2 (7.7%)	8 (25.8%)	4 (19.0%)
3	1 (3.8%)	19 (61.3%)	6 (28.6%)
ADC value (10^{-3} mm^2/s) [b]			
Range	0.34 - 1.51	0.83 - 3.03	0.52 - 2.77
Mean ± SD	0.65 ± 0.24	2.11 ± 0.69	2.07 ± 0.80

[a] ILSS = intralesional susceptibility signal.
[b] ADC = apparent diffusion coefficient.

2.2. MR imaging protocol and processing

The MR imaging examinations were performed using a 1.5-T scanner (Signa; GE Medical System, Milwaukee, WI). All 78 patients underwent MR imaging studies, including transverse T1 spin-echo pre- and post-gadolinium injection (TR/TE = 500/15 ms), transverse T2-weighted fast spin-echo (TR/TE = 4000/100 ms), transverse T2-weighted fluid-attenuated inversion recovery (TR/TE/TI = 9000/120/2200 ms) with section thickness = 5 mm and FOV = 24 cm. Diffusion imaging was performed by using single-shot spin-echo echo-planar imaging (TR/TE = 10,000/93 ms; diffusion sensitivities of b = 0 and 1000s/mm^2; acquisition matrix = 256 × 128; slice thickness = 5 mm; FOV = 24 cm). For SWI, a transverse 3D spoiled gradient-echo sequence with velocity compensation gradients was used (TR/TE = 50/39 ms; acquisition matrix = 288 × 256 × 28; flip angle = 18°; slice thickness = 2.5 mm; FOV = 22 cm). In addition, the contrast-enhanced 3D T1-weighted imaging was collected after administration of gadolinium-based contrast agent by using an inversion-recovery spoiled gradient echo sequence (TE/TR/TI = 4.2/9.2/400 ms; flip angle = 20°; acquisition matrix = 288 × 160 × 124; slice thickness = 1.2 mm; FOV = 24 cm).

Following image acquisition, generation of the trace ADC maps was done based on pixel-by-pixel computation using the Stejskal–Tanner equation, where the signals after adding diffusion-sensitizing gradients were subtracted from those in the b = 0 images after taking the natural logarithm, and then divided by the b-value difference [17]. Analysis of diffusion changes was performed using the manufacturer-provided Functool Performance software (General Electric Medical System). Average ADC in the lesion was calculated by manually contouring the cavity and mean value extracted. For SWI, image processing was executed offline using customized software following the procedure described in the literature [18,19]. In short, a high-pass filter (2D Gaussian with full-width-at-half-maximum = 32 cycles per FOV) was first applied to the phase images to remove background field inhomogeneity near air-tissue interfaces [20], and normalized to create a phase mask where regions with the presence of paramagnetic substances showed a numerical rating between 0 and 1. This normalized phase mask was then multiplied four times with the original magnitude image to further enhance the hypointensity of paramagnetic substances against the surrounding tissues on the final post-processed SWI.

2.3. SWI ILSS data analysis

Three observers (P.H.L., J.H.F., P.C.W.) independently assessed the degree of the ILSS seen on SWI for the rim-enhancing lesions. The ILSS was defined as the presence of either tubular or dot-like hypointense structures seen on SWI. Then on the single imaging slice that visually showed the maximum number of ILSS within the mass, the degree of ILSS was established using a four-grade system based on simple counting of the number of ILSS: Grade 0 was defined as no ILSS; Grade 1 as 1–5 ILSSs; Grade 2 as 6–10 ILSSs; and Grade 3 as ≥11 ILSSs [12–14]. Fuzzy or diffuse low signals, which appeared as mild hypointense or mixed iso- to mild hypointense rim on SWI [21], were not included when counting the number of ILSS (Fig. 1), because the quantification of these findings could be subjective [22]. None of all 78 cases collected in this study had intralesional calcifications that could cause similar findings to the ILSS.

2.4. Statistical analysis

Inter-observer agreement on ILSS grading was assessed using Kendall's coefficient of concordance (KCC). Intra-observer reliability for the three raters was estimated using both Cohen's quadratic-weighted kappa and intraclass correlation coefficient (ICC), by repeating ILSS grading at least two weeks apart on five cases randomly selected from each of the three disease categories (total 15 cases repeated per rater).

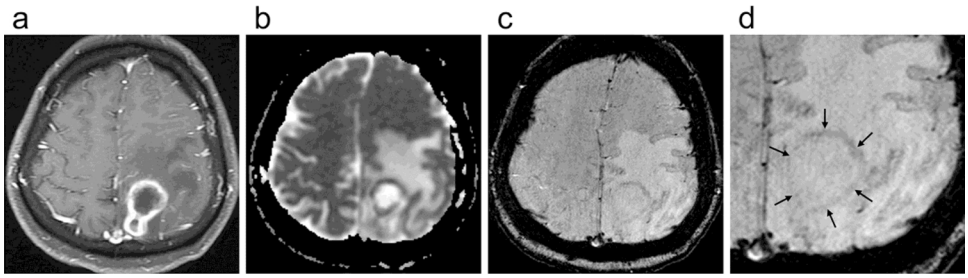

Fig. 1. A 27-year-old male patient with pyogenic brain abscess.
a. Contrast-enhanced T1-weighted image demonstrates rim-enhancing mass.
b. ADC map shows high signal intensity in the cavity of abscess like that of cerebrospinal fluid, reflecting the exception of marked diffusion (1.51×10^{-3} mm^2/s). c. High-resolution SWI shows no ILSS (Grade 0) within the mass.
d. The magnified view of c reveals somewhat fuzzy and diffuse low signals (arrows), which are excluded in the counting of ILSS.

ROC curve analyses were used to compare the difference between abscesses and two rim-enhancing necrotic tumors, i.e., abscesses versus glioblastomas and abscesses versus metastases, when using ILSS alone, ADC alone, or ILSS and ADC combined (termed the ILSS-ADC combined model). For the ILSS-ADC combined model, logistic regression was applied to first obtain the prediction probability, which was then used to derive the ROC curve. The areas under the ROC curves (AUCs) representing the disease differentiation abilities using ILSS and/or ADC were then compared using the DeLong, DeLong, and Clarke–Pearson method [23], which is a nonparametric approach to compare areas under correlated ROC curves, by using the generalized U-statistics to generate an estimated covariance matrix. The cutoff value for classification based on continuous variables was the value yielding the maximum sum of sensitivity and specificity. Diagnostic accuracy, sensitivity, specificity, positive predictive value, and negative predictive value were subsequently derived and reported. These analyses were carried out using SPSS software (IBM SPSS statistics v.19, Armonk, NY) and the MedCalc statistical package (MedCalc Software, Ostend, Belgium), with the level of statistical significance set at $P < 0.05$.

3. Results

The distributions of ILSSs and ADCs in each type of rim-enhancing lesion are summarized in Table 1. Inter-observer agreement for ILSS grading was good, showing a KCC of 0.92, making operator dependence a minor concern. In addition, the intra-observer reliability of rater 1, 2, and 3 was 1, 1, and 0.972 by Cohen's quadratic-weighted kappa and 1, 1, and 0.974 by ICC, respectively, all showing very high consistency. In ILSS analysis, a low degree of ILSS (ILSS Grade 0, 46.2% and Grade 1, 42.3%) was in most of the abscess group. A high degree of ILSS (ILSS Grade 3, 61.3%) was in most of the glioblastoma group. ILSS tended to spread relatively evenly for the metastatic group, in which Grade 0 (33.3%) and Grade 3 (28.6%) each accounted for about one-third of ILSS. As to the diffusion behavior, although the ADC values for the abscess group were generally smaller than the other two groups, substantial overlap in the ADC ranges indicated that some exceptions were present as demonstrated in Figs. 1 and 2. In the two cases shown, ILSS grades complemented ADC for differential diagnosis.

The results of ROC analysis in differentiating abscess from glioblastoma and abscess from metastasis are summarized in Table 2 and Fig. 3. The ILSS-ADC combined model had greater AUCs than ILSS or ADC used alone in both cases. In particular, the ILSS-ADC combined model showed 100% diagnostic accuracy differentiating abscesses from glioblastoma, although the improvement versus the ADC model did not reach statistical significance ($P = 0.157$) likely due to limited number of cases showing atypical ADC behavior. The perfect differentiation between abscesses and glioblastoma is further shown in a 2D graph (Fig. 4), where a manually drawn line can be seen to completely separate the two groups of patients. On the other hand, the ADC model and the ILSS-ADC combined model performed equally well in distinguishing abscesses from metastases.

4. Discussion

SWI is known to be sensitive to paramagnetic blood products and venous vasculature that manifest as darkened spots on an image. Since high-grade gliomas with active angiogenesis often result in a relatively large amount of deoxyhemoglobin, increased signal loss on SWI is indicative of conglomerates of tumor microvascularity [24]. As a result, the use of intratumoral susceptibility signals on SWI has been shown to be a helpful tool for non-invasive glioma grading [13,19,24,25]. On the other hand, for rim-enhancing masses including brain abscesses, an earlier study [12] reported that when using SWI alone, the degree of ILSS may contribute to the differential diagnosis, showing diagnostic accuracy (88.1%) in distinguishing abscesses from glioblastomas, in distinguishing abscesses from metastases (68.2%), and in distinguishing glioblastomas from metastases (70.5%) [12]. These findings are understandable, because in experimental settings, brain abscesses exhibit relatively high amounts of mature collagen and consequently decreased neovascularity [26,27]. Thus, the lack of ILSSs in abscesses could be attributed to the rarity of vascularity. Nonetheless, it is clear that SWI alone is considered inadequate in differentiating abscesses from brain tumors. Noting that DWI and SWI are showing image contrasts based on completely different mechanisms, we thus sought to investigate whether the combined use of indices derived from DWI and SWI, namely the quantitative ADC and the semi-quantitative ILSS, could further assist the differential diagnosis between these rim-enhancing masses. To the best of our knowledge, similar studies integrating ILSS and DWI for the differential diagnosis of rim-enhancing lesions have not been reported before.

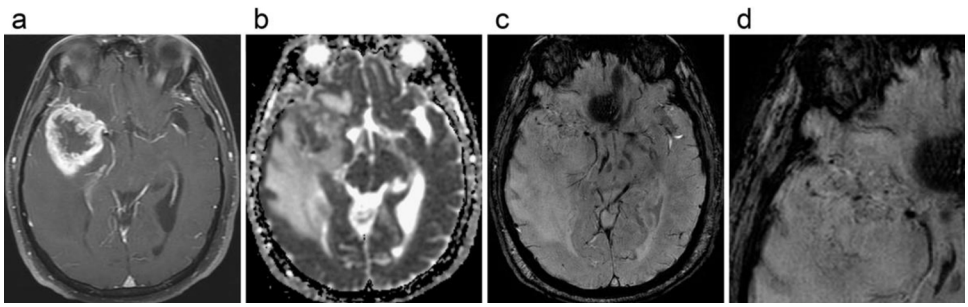

Fig. 2. A 61-year-old male patient with necrotic glioblastoma.
a. Contrast-enhanced T1-weighted image demonstrates rim-enhancing mass.
b. ADC map shows low signal intensity in the cavity of necrotic glioblastoma reflecting the exception of restricted diffusion (0.95×10^{-3} mm^2/s).
c. High-resolution SWI shows high-grade ILSS (Grade 3).
d. The magnified view of c shows multiple linear and dot-like structures within the mass.

Table 2
Diagnostic accuracies of ILSS, ADC, and ILSS-ADC combined model in differentiating abscess from glioblastoma and abscess from metastasis.

	Criterion	Accuracy, %	Sensitivity, %	Specificity, %	PPV, %	NPV, %	AUC
Abscess *vs.* Glioblastoma							
ILSS **	< 2 [a]	87.7 (76.3–94.9)	88.5 (69.8–97.6)	87.1 (70.2–96.4)	85.2 (66.3–95.8)	90.0 (73.5–97.9)	0.91 (0.81–0.97)
ADC **	≦0.78 [b]	94.7 (85.4–98.9)	88.5 (69.8–97.6)	100 (88.8–100)	100 (85.2–100)	91.2 (76.3–98.1)	0.98 (0.90–1.00)
ILSS and ADC **	> 7.80E-07 [c]	100 (86.8–100)	100 (86.8–100)	100 (88.8–100)	100 (86.8–100)	100 (88.8–100)	1.00 (0.94–1.00)
Abscess *vs.* Metastasis							
ILSS *	< 2 [a]	70.2 (55.1–82.7)	88.5 (69.8–97.6)	47.6 (25.7–70.2)	67.6 (49.5–82.6)	76.9 (46.2–95.0)	0.71 (0.56–0.84)
ADC **	≦0.78 [b]	91.5 (79.6–97.6)	88.5 (69.8–97.6)	95.2 (76.2–99.9)	95.8 (78.3–99.9)	87.0 (66.4–97.2)	0.95 (0.84–0.99)
ILSS and ADC **	> 0.1497 [c]	91.5 (76.9–96.5)	100 (86.8–100)	81.0 (58.1–94.6)	86.7 (68.9–96.4)	100 (80.5–100)	0.97 (0.88–1.00)

The 95% confidence interval is in parenthesis.
ILSS = intralesional susceptibility signal; ADC = apparent diffusion coefficient ($\times 10^{-3}$ mm^2/s); PPV = positive predictive value; NPV = negative predictive value; AUC = area under the receiver operating characteristics curve.
* $P < 0.05$.
** $P < 0.001$.
[a] ILSS grade.
[b] ADC value.
[c] Probability of combined model.

The most important finding from our study is perhaps the encouraging 100% accuracy differentiating abscesses from glioblastoma when using ILSS and ADC information combined together. This result, in our opinion, should be valuable to the radiological community, as there have been no similar reports in the current literature. There are some articles documenting the combined use of DWI and SWI to characterize brain abscesses [28–30], yet in ways rather different from our approach. Gupta et al. investigated 15 patients with histologically-proven brain abscess, in which 11 were histopathologically found to have hemorrhage in the abscess wall but without quantifying their ILSS grades on SWI [28]. Among the three cases whose images were shown in that study, one demonstrated presence of ILSS likely with grade 1 or 2, whereas the other two showed absence of ILSS (grade 0). [28] In another study, prominent signal loss on SWI likely corresponding to ILSS grade 3 was identified in the lesion cores in a series of three cases of pyogenic brain abscess [29]. The article by Antulov et al. also reported DWI and SWI behavior of ten pyogenic abscesses [30], but focusing on the presence of the dual-rim sign on SWI [31] rather than ILSS. In the three previously mentioned studies [28–30], however, all DWI images shown in these articles exhibited the typical behavior of restricted diffusion in the abscess cavities, meaning that differentiation from glioblastoma using ADC alone would suffice. In such cases, ILSS grades would demonstrate no additional usefulness in differential diagnosis, except for lesion characterization value.

The excellent performance of the ILSS-ADC combined model found in our cases strongly suggests that SWI and DWI provide mutually complementary microscopic information in these rim-enhancing lesions, particularly for patients showing atypical DWI behavior. As opposed to the typical presence of serous liquid of high ADC within the necrotic core [3–6,8], glioblastoma that exhibits atypical restricted diffusion was attributed to factors including intratumoral microhemorrhage [10]. In this regard, therefore, the ILSS grade may assist ADC in differential diagnosis at least for glioblastoma. On the other hand, the atypically high ADC in brain abscesses could have originated from a variety of reasons such as variable concentrations of inflammatory cells and bacteria, different etiological organisms, prominent necrotic debris, and so forth [7]. Documentations on their possible linkage with microhemorrhage to result in low signals on SWI, however, were currently unavailable. Hence the additive value of ILSS grade to confirm the diagnosis of pyogenic abscesses with atypically

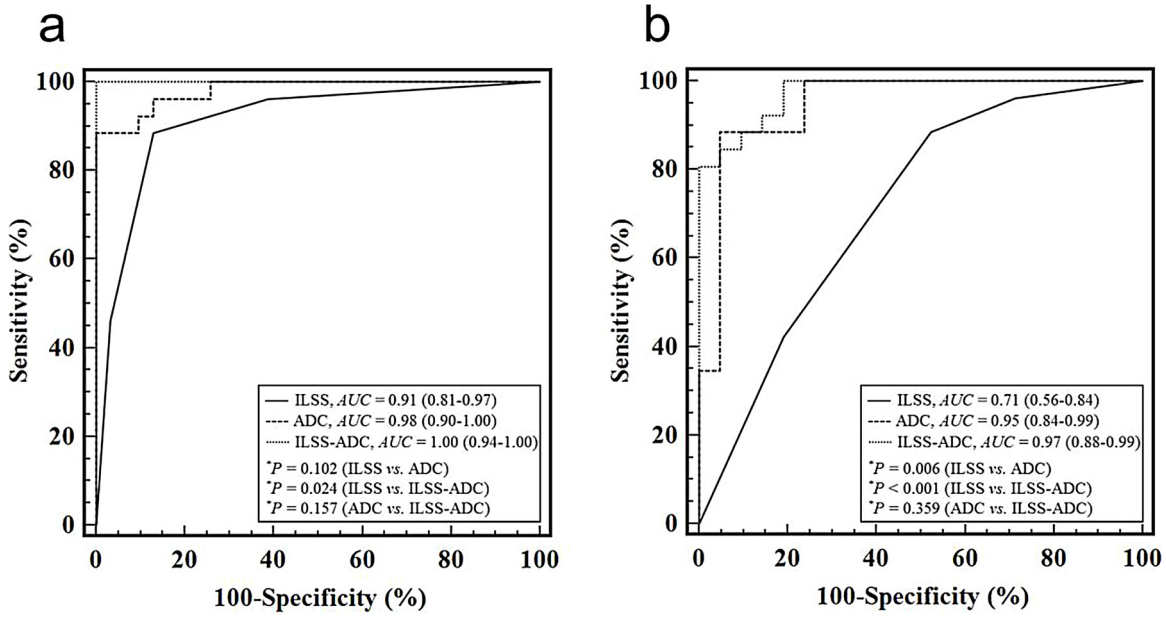

Fig. 3. ROC curve of logistic regression model for predicting the probability of occurrence of Disease in Disease vs. Reference. (a) Abscess vs. Glioblastoma, (b) Abscess vs. Metastasis. AUCs of any two methods are compared using DeLong, DeLong, and Clarke–Pearson method.

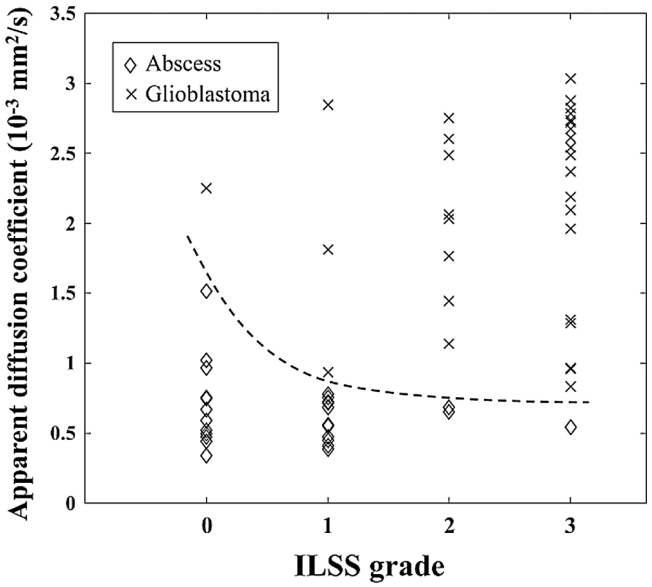

Fig. 4. 2D plot showing complete separation of abscesses from glioblastoma with ADC and ILSS for patients included in this study. The dashed line is manually drawn just to demonstrate the differentiation schematically.

high ADC remains unknown. Future investigations with regional radiological-pathological correlation to microscopically unravel the roles of SWI and DWI would be necessary to address these unsolved issues related to the complex interactions between hemorrhage and ADC, which was unfortunately not accomplished in our study due to the retrospective nature.

Exciting as it may appear to be, the 100% differentiation of abscesses from glioblastoma reported in our study has one critical limitation that needs to be noted. The sample size of abscesses and tumor pathologies was small, which precludes direct extrapolation of our results to general situations encountered in daily clinical practice. In particular, the incremental improvements in differential diagnosis introduced by integrating ILSS grades to ADC were rather minor, because differentiation between abscesses and glioblastoma using solely the ADC criteria was hampered only by the presence of few abscess/glioblastoma patients showing atypically high/low ADC. Therefore, it is not impossible that the perfect differentiation in our study happened to be incidental. In this regard, validation of our results by independent cohorts is very important. Nevertheless, since abscesses/glioblastoma patients with atypical ADC behavior were rather infrequent [5,8,32], the potential importance of ILSS should not be neglected simply due to lack of statistical power in our patients. We hope that the presentation of our preliminary findings in this article could raise the attention of other investigators to start looking into the effectiveness of the ILSS-ADC combined model by collaboratively collecting cases showing intracranial rim-enhancing lesions, especially for abscesses/glioblastoma patients demonstrating atypical ADC behavior [7,10].

Our study has one more limitation that needs to be addressed. Despite the usefulness of ILSS in complementing ADC for differential diagnosis between abscesses and glioblastoma, differentiation of necrotic metastasis from other types of rim-enhancing lesions remains difficult. This limitation is further complicated by the fact that most of the metastatic tumor pathologies investigated in our current study are of lung cancer. In other words, only a limited variety of metastases was studied, with trends heavily weighed by lung metastasis. Inclusion of metastases of different histopathologic origins may alter the results regarding differential diagnostic accuracy.

In conclusion, SWI and ADC are complementary, and the combination of SWI and ADC may improve results compared with the use of only one technique to differentiate between abscesses, necrotic glioblastomas, and necrotic metastatic brain tumors. At this stage, SWI and ADC show promise for the non-invasive differentiation of pyogenic brain abscesses from necrotic glioblastomas and necrotic metastatic brain tumors; however, these findings should be addressed and further validated in future clinical studies.

Conflict of interest

All of the authors and authors' institutions have no conflicts of interest.

Declarations of interest

None.

Funding

The study has been supported in part from the Ministry of Science and Technology (MOST) research grants (103-2314-B-075B-001, 104-2314-B-075B-004-MY2, 104-2221-E-110-039, 105-2221-E-002-142-MY3) and from Kaohsiung Veterans General Hospital (VGHKS105-115, VGHKS106-136) in Taiwan.

Acknowledgments

We thank Chia-Chi Hsiao, RT, and Hung-Chieh Huang, RT, for patient MRI scanning, Chiu-Ya Wang, RN, for patient preparation, and research assistants Ya-Hsin Cheng, Tseng-Jui Hsu, for data management.

References

[1] D.W. Lau, N.C. Klein, B.A. Cunha, Brain abscess mimicking brain tumor, Heart Lung 18 (6) (1989) 634–637.
[2] A.N. Mamelak, T.J. Mampalam, W.G. Obana, M.L. Rosenblum, Improved management of multiple brain abscesses: a combined surgical and medical approach, Neurosurgery 36 (1) (1995) 76–85 discussion 85–86.
[3] Y.J. Kim, K.H. Chang, I.C. Song, H.D. Kim, S.O. Seong, Y.H. Kim, M.H. Han, Brain abscess and necrotic or cystic brain tumor: discrimination with signal intensity on diffusion-weighted MR imaging, AJR Am. J. Roentgenol. 171 (6) (1998) 1487–1490.
[4] K. Noguchi, N. Watanabe, T. Nagayoshi, T. Kanazawa, S. Toyoshima, M. Shimizu, H. Seto, Role of diffusion-weighted echo-planar MRI in distinguishing between brain brain abscess and tumour: a preliminary report, Neuroradiology 41 (3) (1999) 171–174.
[5] S.C. Chang, P.H. Lai, W.L. Chen, H.H. Weng, J.T. Ho, J.S. Wang, C.Y. Chang, H.B. Pan, C.F. Yang, Diffusion-weighted MRI features of brain abscess and cystic or necrotic brain tumors: comparison with conventional MRI, Clin. Imaging 26 (4) (2002) 227–236.
[6] P.H. Lai, J.T. Ho, W.L. Chen, S.S. Hsu, J.S. Wang, H.B. Pan, C.F. Yang, Brain abscess and necrotic brain tumor: discrimination with proton MR spectroscopy and diffusion-weighted imaging, AJNR Am. J. Neuroradiol. 23 (8) (2002) 1369–1377.
[7] E.J. Lee, K.J. Ahn, Y.S. Ha, H.E. Oh, C.S. Park, S.Y. Song, N.H. Park, M.S. Kim, Unusual findings in cerebral abscess: report of two cases, Br. J. Radiol. 79 (947) (2006) e156–61.
[8] J.S. Reddy, A.M. Mishra, S. Behari, M. Husain, V. Gupta, M. Rastogi, R.K. Gupta, The role of diffusion-weighted imaging in the differential diagnosis of intracranial cystic mass lesions: a report of 147 lesions, Surg. Neurol. 66 (3) (2006) 246–250 discussion 250–251.
[9] M. Hartmann, O. Jansen, S. Heiland, C. Sommer, K. Munkel, K. Sartor, Restricted diffusion within ring enhancement is not pathognomonic for brain abscess, AJNR Am. J. Neuroradiol. 22 (9) (2001) 1738–1742.
[10] B. Hakyemez, C. Erdogan, N. Yildirim, M. Parlak, Glioblastoma multiforme with atypical diffusion-weighted MR findings, Br. J. Radiol. 78 (935) (2005) 989–992.
[11] P.H. Lai, S.S. Hsu, S.W. Ding, C.W. Ko, J.H. Fu, M.J. Weng, L.R. Yeh, M.T. Wu, H.L. Liang, C.K. Chen, H.B. Pan, Proton magnetic resonance spectroscopy and diffusion-weighted imaging in intracranial cystic mass lesions, Surg. Neurol. 68 (Suppl. 1) (2007) S25–36.
[12] J.H. Fu, T.C. Chuang, H.W. Chung, H.C. Chang, H.S. Lin, S.S. Hsu, P.C. Wang, S.H. Hsu, H.B. Pan, P.H. Lai, Discriminating pyogenic brain abscesses, necrotic glioblastomas, and necrotic metastatic brain tumors by means of susceptibility-weighted imaging, Eur. Radiol. 25 (5) (2015) 1413–1420.
[13] M.J. Park, H.S. Kim, G.H. Jahng, C.W. Ryu, S.M. Park, S.Y. Kim, Semiquantitative assessment of intratumoral susceptibility signals using non-contrast-enhanced high-field high-resolution susceptibility-weighted imaging in patients with gliomas: comparison with MR perfusion imaging, AJNR Am. J. Neuroradiol. 30 (7) (2009)

1402–1408.
[14] S.M. Park, H.S. Kim, G.H. Jahng, C.W. Ryu, S.Y. Kim, Combination of high-resolution susceptibility-weighted imaging and the apparent diffusion coefficient: added value to brain tumour imaging and clinical feasibility of non-contrast MRI at 3 T, Br. J. Radiol. 83 (990) (2010) 466–475.
[15] J.R. Reichenbach, R. Venkatesan, D.J. Schillinger, D.K. Kido, E.M. Haacke, Small vessels in the human brain: MR venography with deoxyhemoglobin as an intrinsic contrast agent, Radiology 204 (1) (1997) 272–277.
[16] J.R. Reichenbach, E.M. Haacke, High-resolution BOLD venographic imaging: a window into brain function, NMR Biomed. 14 (7–8) (2001) 453–467.
[17] E.O. Stejskal, J.E. Tanner, Spin diffusion measurements: spin echoes in the presence of a time-dependent field gradient, J. Chem. Phys. 42 (1) (1965) 288–292.
[18] E.M. Haacke, S. Mittal, Z. Wu, J. Neelavalli, Y.C. Cheng, Susceptibility-weighted imaging: technical aspects and clinical applications, part 1, AJNR Am. J. Neuroradiol. 30 (1) (2009) 19–30.
[19] S. Mittal, Z. Wu, J. Neelavalli, E.M. Haacke, Susceptibility-weighted imaging: technical aspects and clinical applications, part 2, AJNR Am. J. Neuroradiol. 30 (2) (2009) 232–252.
[20] H.C. Chang, T.C. Chuang, H.W. Chung, H.S. Lin, P.H. Lai, M.J. Weng, J.H. Fu, P.C. Wang, S.C. Li, H.B. Pan, Multilayer appearance on contrast-enhanced susceptibility-weighted images on patients with brain abscesses: possible origins and effects of postprocessing, J. Magn. Reson. Imaging 36 (6) (2012) 1353–1361.
[21] P.H. Lai, H.C. Chang, T.C. Chuang, H.W. Chung, J.Y. Li, M.J. Weng, J.H. Fu, P.C. Wang, S.C. Li, H.B. Pan, Susceptibility-weighted imaging in patients with pyogenic brain abscesses at 1.5T: characteristics of the abscess capsule, AJNR Am. J. Neuroradiol. 33 (5) (2012) 910–914.
[22] H.S. Kim, G.H. Jahng, C.W. Ryu, S.Y. Kim, Added value and diagnostic performance of intratumoral susceptibility signals in the differential diagnosis of solitary enhancing brain lesions: preliminary study, AJNR Am. J. Neuroradiol. 30 (8) (2009) 1574–1579.
[23] E.R. DeLong, D.M. DeLong, D.L. Clarke-Pearson, Comparing the areas under two or more correlated receiver operating characteristic curves: a nonparametric approach, Biometrics 44 (3) (1988) 837–845.
[24] K. Pinker, I.M. Noebauer-Huhmann, I. Stavrou, R. Hoeftberger, P. Szomolanyi, G. Karanikas, M. Weber, A. Stadlbauer, E. Knosp, K. Friedrich, S. Trattnig, High-resolution contrast-enhanced, susceptibility-weighted MR imaging at 3T in patients with brain tumors: correlation with positron-emission tomography and histopathologic findings, AJNR Am. J. Neuroradiol. 28 (7) (2007) 1280–1286.
[25] C. Li, B. Ai, Y. Li, H. Qi, L. Wu, Susceptibility-weighted imaging in grading brain astrocytomas, Eur. J. Radiol. 75 (1) (2010) e81–5.
[26] R.H. Britt, D.R. Enzmann, A.S. Yeager, Neuropathological and computerized tomographic findings in experimental brain abscess, J. Neurosurg. 55 (4) (1981) 590–603.
[27] N.P. Ferreira, G.M. Otta, L.L. do Amaral, A.J. da Rocha, Imaging aspects of pyogenic infections of the central nervous system, Top. Magn. Reson. Imaging 16 (2) (2005) 145–154.
[28] R.K. Gupta, V. Tomar, R. Awasthi, A. Yadav, N. Husain, V. Bharadwaj, B.K. Ojha, S. Behari, K.N. Prasad, R.K. Rathore, T2*-weighted MR angiography substantially increases the detection of hemorrhage in the wall of brain abscess: implications in clinical interpretation, Neuroradiology 54 (6) (2012) 565–572.
[29] K. Thamburaj, A.K. Agarwal, S.B. Sabat, D.T. Nguyen, Hemorrhage in the wall of pyogenic brain abscess on susceptibility weighted MR sequence: a report of 3 cases, Case Rep. Radiol. 2014 (2014) 907584.
[30] R. Antulov, K. Dolic, J. Fruehwald-Pallamar, D. Miletic, M.M. Thurnher, Differentiation of pyogenic and fungal brain abscesses with susceptibility-weighted MR sequences, Neuroradiology 56 (11) (2014) 937–945.
[31] C.H. Toh, K.C. Wei, C.N. Chang, P.W. Hsu, H.F. Wong, S.H. Ng, M. Castillo, C.P. Lin, Differentiation of pyogenic brain abscesses from necrotic glioblastomas with use of susceptibility-weighted imaging, AJNR Am. J. Neuroradiol. 33 (8) (2012) 1534–1538.
[32] C.H. Toh, K.C. Wei, S.H. Ng, Y.L. Wan, C.P. Lin, M. Castillo, Differentiation of brain abscesses from necrotic glioblastomas and cystic metastatic brain tumors with diffusion tensor imaging, AJNR Am. J. Neuroradiol. 32 (9) (2011) 1646–1651.